DOI: https://doi.org/10.1016/j.matdes.2022.111052

Materials & Design 222 (2022) 111052

Contents lists available at ScienceDirect

Materials & Design

journal homepage: www.elsevier.com/locate/matdes

Quality index for friction stir welds in 7050 aluminum plates

Shirley Alexandra Garcia Ruano *, Auteliano Antunes dos Santos Junior

School of Mechanical Engineering, University of Campinas, 200 Rua Mendeleyev, Campinas 13083860, SP Brazil

HIGHLIGHTS

- A quality index QI-FSW based on residual stresses is proposed and can identify the best set of welding parameters.
- FSW joints at 400 mm/min showed the worst quality and at 200 mm/min, the best.
- Maximum equivalent residual stress (ERS) was 250 MPa, 50% of AA7050 Yield Strength.
- Plates welded with same parameters show residual stress distributions with M shapes.
- Maximum stress between 149 MPa and 356 MPa were found close to the weld center.

GRAPHICAL ABSTRACT

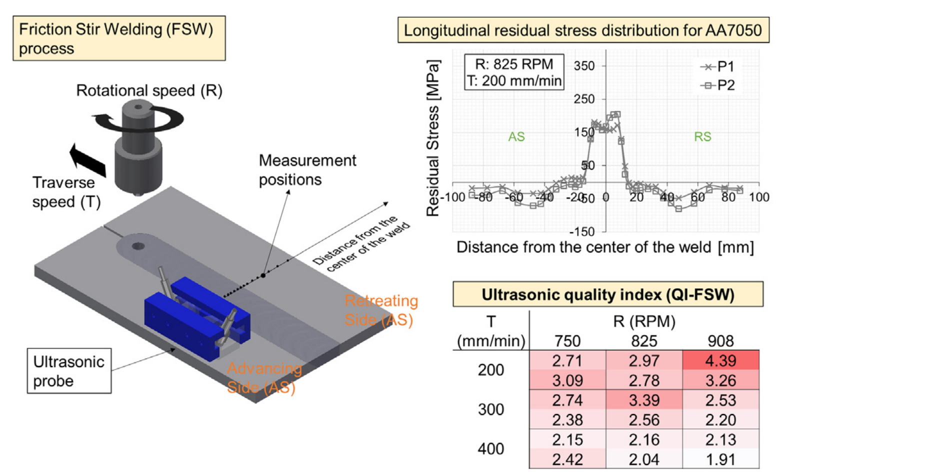

ARTICLE INFO

Article history:
Received 10 March 2022
Revised 3 August 2022
Accepted 8 August 2022
Available online 18 August 2022

Keywords:
Non-destructive testing
Quality index
Residual stress
Ultrasonic method
Friction stir welding
Aluminum alloy

ABSTRACT

AA7050-T7451 is a heat-treating aluminum alloy with high mechanical strength, ideal for producing lightweight structural components. Common types of welding lead to structural changes in the material that could decrease their mechanical properties affecting the fatigue life of the joints; however, a solid-state process known as friction stir welding (FSW) have been increasingly used as an alternative solution to reduce these severe effects. This work attempts to study the FSW behavior over 7050-T7451 aluminum alloys through the characterization of the resulting residual stresses and propose a manufacturing quality index based on their magnitude and distribution. An ultrasonic method employing longitudinal critically refracted (LCR) waves was used to determine the longitudinal residual stresses at different distances from the centerline in plates welded with different parameters.The resulting stress distribution is consistent with the literature review, presenting maximum values around 200 MPa at the center of the weld. A quality index was calculated through the average of all stresses in that region. It was found that higher residual stresses are produced with higher traverse and rotational speed (400 mm/min and 908 RPM). Therefore, to improve the process regarding the level of residual stresses, it is recommended to use lower welding tool velocities.

1. Introduction

The critical design parameters and requirements from the aeronautical industry, have been motivated the development of high tenacity and low weight materials [1]. Despite polymer matrix

* Corresponding author.
E-mail address: shirleyruano@fem.unicamp.br (S.A. Garcia Ruano).

https://doi.org/10.1016/j.matdes.2022.111052
0264-1275/© 2022 The Authors. Published by Elsevier Ltd.

composites are increasingly being used for some applications in modern commercial aircrafts, aluminum alloys remain the primary choice for the fuselage, wing and support structures of commercial, cargo and military transport airplanes. [2–4].

Alloy 7050-T74 was developed to meet the demand for lightweight high strength materials with good resistance to stress corrosion, fracture and fatigue. Its most notorious applications is in the aeronautical industry, where it is present in the spars of horizontal and vertical stabilizers of aircraft [5]. 7XXX series alloys contain zinc in amounts from 1 to 8% of mass concentration, combined with a lower percentage of magnesium results in an intermetallic compound $MgZn_2$ which increases the hardness of the alloy during precipitation heat treatment. In addition, 7050 alloy has a higher copper content, which improves corrosion resistance but decrease its weldability [6,7]. This alloy could undergo phase segregation during melt welding; and the temperature increase in the surrounding areas can produce precipitate dissolution in the metallic matrix, causing overaging and inducing the formation of cracks at high temperatures (mainly during solidification) [8,9]. These metallurgical changes make conventional fusion welding processes difficult, requiring the application of previous treatments to achieve adequate joints [10]. Another alternative to integrate welding processes in this kind of alloys is through the use of solid-state welding processes, like the FSW, which is the focus of this study.

The main parameters to be considered for this type of welding are the rotation and traverse speeds of the tool. Most works study the evolution of the mechanical properties of the welded joint as a function of axial forces, tool geometry, and tilt angle, all of which must be also properly selected to assure union quality [11–14]. All those parameters, along with the physical characteristics of the tool, depend on the material alloy properties and its dimensions according to each application, so it could be harder to determine them separately.

Several authors have evaluated the process based on the resulting mechanical properties of the joint, the micro-structural analysis and others characterization methods, like fatigue tests [15–17]. One of the influencing factors in the performance of welded joints is the presence of residual stresses. The development of residual stresses in welded parts and structures can generate several problems, such as the formation of cracks, greater propensity for the occurrence of fatigue or fragile fracture, and loss of dimensional stability [18–20]. Knowing the magnitude and distribution of these stresses within the material would contribute to the study of fatigue behavior and lifetime and would serve to characterize the process for the welded material.

In recent studies, several measurement techniques have been tested for the evaluation of residual stresses, which can be classified into destructive methods, based on mechanical stress relaxation like sectioning or hole-drilling; and non-destructive testing (NDT), based on physical or crystallographic characteristics that change with the variation of the internal stresses in the material [21–23]. The most known NDT techniques are X-ray diffraction, neutron diffraction, ultrasonic, and magnetic techniques [24–26].

The use of the ultrasonic method for residual stress determination has been tested in many different applications; a procedure using critically refracted longitudinal waves (LCR), tested initially on railroads [27], has been proved suitable for welding evaluation by some authors [28–33]. It is an emission and reception method, that consists of measuring the travel time - TOF (Time-of-flight) of the LCR wave propagating between two or more transducers positioned in a specific configuration. The stress determination is based on the acoustoelastic effect, which describes how the variation of the speed of the elastic waves propagating in solids is subject to the state of stress within the material. Considering the classical approach of small deformations, this relation could be linear and expressed through an acoustoelastic coefficient.

This work studies the welding quality for 7050 aluminum plates joined by FSW, through the analysis of their residual stresses measured using the ultrasonic method. As far as we know, the technique has not be used to measure stresses in this alloy, though some authors use ultrasound for other kinds of evaluation [34,35]. To perform these measurements, we use an improved system that was tested in a previous study for 5052 aluminum alloy, in which the accuracy of the results was validated by the hole-drilling method [36]. The FSW parameters were found considering the characteristics of the material, then the plates are welded for different tool speeds. Thus, the residual stresses are related to each speed and a quality index is proposed. As long as the integrity of the plates was verified, the quality of the process can be related to this parameter, which would allow optimizing the process in future applications. Besides, this quality index can be used as a control tool at the end of the process, ensuring the safety of using the structure in service.

2. Methods

The measurement procedures are described in this section. To establish the proper quality index, several experiments were carried out.

At first, the plates are shaped to 5 mm thick, 10 mm wide, and 30 mm long. They are butt joined in pairs. The principal process parameters for FSW are schematically represented in Fig. 1. For this study, the rotational (R) and traverse (T) speeds are the independent variables for the welding experiments design. The downward force is an indispensable parameter to ensure a full penetration; however, the present evaluation is performed on fully welded joints free of defects. For this reason, the force and other welding parameters remain constant after being previously determined in a set of preliminary experiments.

Before welding, some measurements were also taken, as will be described in the following subsection. Then, the plates are welded obeying a factorial design with central variables and two replications per combination, as shown in Table 1, where 825 RPM and 300 mm/min are considered as central parameters. A tilt angle of 1.5°, and downward axial force of 18.5 kN were used for all cases. The plates are identified with the letter P and an exclusive number.

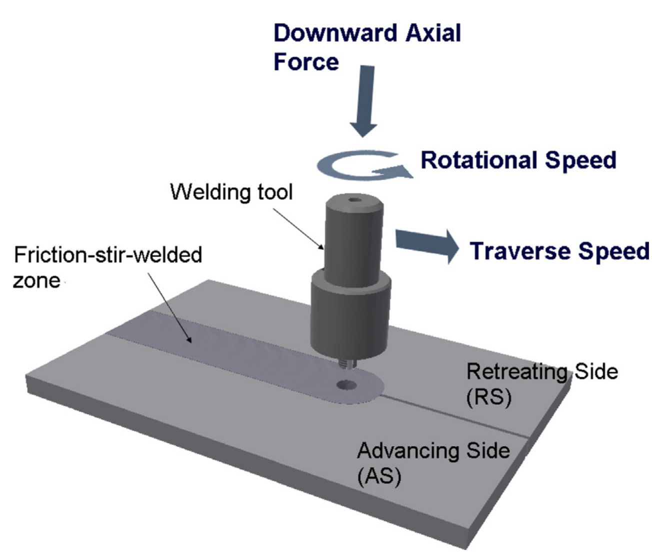

Fig. 1. Schematic representation of FSW and principal process parameters.

Table 1
FSW parameters combinations.

	Rotational Speed (R) RPM		
Traverse Speed (T) mm/min	750	825	908
200	P4, P5	P1, P2	P3, P12
300	P18, P17	P6, P13	P8, P9
400	P7, P11	P15, P10	P16, P14

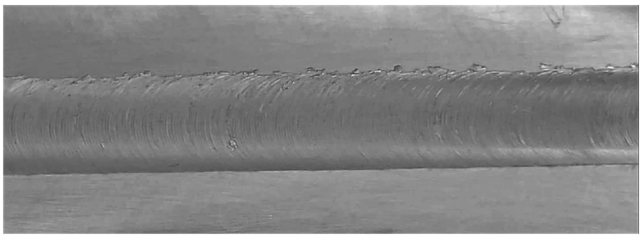

Fig. 2. Fabricated FSW joints, surface appearance.

Plates joined by FSW can be seen in Figure 2. To grant the coupling of the ultrasonic probe with the welded plate, all surfaces are machined, leaving a smooth surface without bumps. After each weld, the internal integrity of the joint is verified by ultrasonic scanning using Phased Arrays. In addition, the cross-section of the weld was evaluated through macrography and micro-hardness analysis.

2.1. Ultrasonic Measurements

The ultrasonic measurement system used in this work is composed of 4 principal devices, as shown in Fig. 3. The ultrasonic probe, designed and tested previously, basically consists of two single-crystal normal-beam ultrasonic transducers of 3.5 MHz coupled to 25° inclination wedges for generating LCR waves. A metallic guide maintains the distance between the wedges fixed. As mentioned above, the ultrasonic system was previously tested [36]. All the components, including the transducers, were calibrated and selected based on the repeatability of the measurements. For this particular setup, the standard deviation for Aluminum Alloys was less than 5 ns.

The stress calculation is based on the acoustoelastic effect, which relates the wave velocity with the stress state inside the material [37,38]. As the distance between the transducers is kept constant, the acoustoelastic relationship between the longitudinal wave velocities directly depends on the time of the wave travel inside the material or time-of-flight (TOF). For isotropic materials, this could be expressed by Eq. 1.

$$\sigma = E\frac{t - t_0}{Lt_{ref}} \tag{1}$$

where σ is the stress to be determined, E is the elasticity modulus, L is the acoustoelastic coefficient of the longitudinal wave propagating in the same direction of the stress, t_{ref} is the theoretical propagation time of the wave inside the material, t_0 is the wave propagation TOF for the stress-free state, and t is the TOF for the current stress state. The term t_{ref} is calculated as the distance between the transducers over the theoretical velocity of the longitude wave in aluminum. Both TOF terms are obtained with the ultrasonic apparatus. Notice that t_0 must be measured on the plates at a stress-free state; for this study, it corresponds to the condition before welding.

The TOF measured by the ultrasonic method is influenced by factors other than stress, like temperature, pressure or texture. Most of them can be kept constant, especially when measurements are made within a laboratory. However, the influence of temperature and surface irregularities were considered in this study. The relationship between temperature and TOF is found to be linear, so a correction factor f_{temp} can be found through a calibration experiment. For this experiment, the temperature was controlled using an air conditioner. Upon stably reaching the lowest

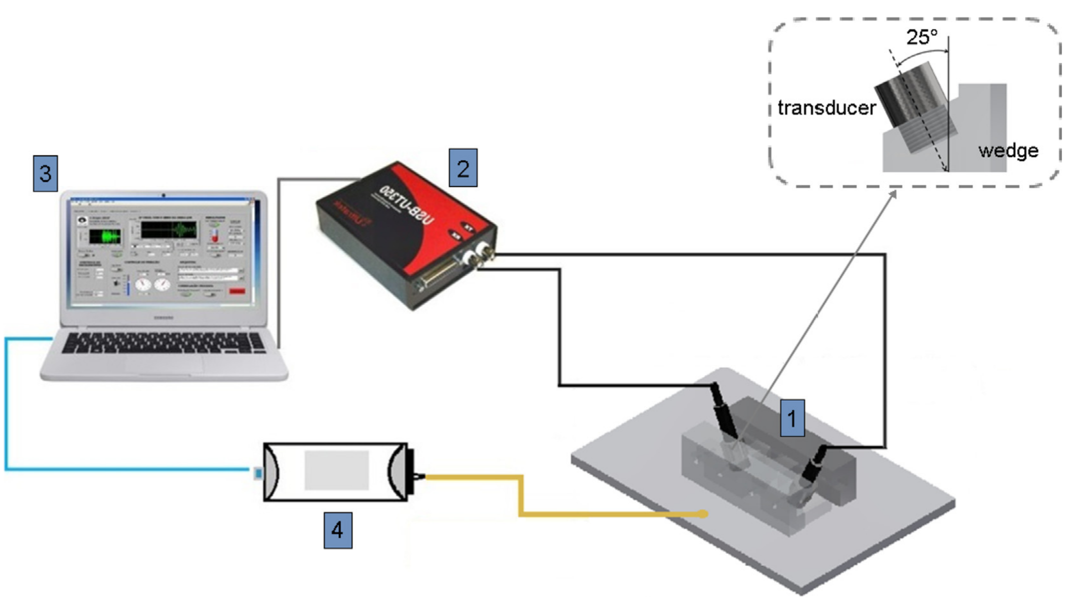

Fig. 3. Ultrasonic Measurement System. (1) Ultrasonic Probe, (2) Pulser-Receiver Device, (3) Computer, (4) Temperature Sensor.

temperature in the room with the ultrasonic system mounted, the air conditioning was turned off and the TOF was recorded, while the temperature gradually increased. Measurements were taken at every 0.5°C measured at the plate with a thermocouple.

To consider the surface finishing or surface texture, measurements were made before and after machining the welded plates. The time difference is considered in the stress-free time as described in expressions 2.

$$\begin{aligned} t &= t^* + f_{temp}(24^\circ - T^\circ) \\ t_0 &= t_0^* + f_{temp}(24^\circ - T^\circ) + (t_{aft} - t_{bef}) \end{aligned} \tag{2}$$

In the expressions above, * represents the TOF measured directly with the ultrasonic probe for both states, T° is the temperature for each measurement and f_{temp} is the correction factor for temperature variation. Notice that the reference is 24°C. Besides, t_{bef} is the TOF measured on the plate in a region far from the welded zone, before machining, and t_{aft} is the TOF afterward in the same position.

The measurement of TOF for the welded plates (t) was carried out every 10 mm or 5 mm in the base material and every 2.5 mm in the welded and nearby zones, Figure 4. The ultrasonic probe is positioned for the direction of wave propagation is parallel to the weld. Therefore, the resulting stress corresponds to the longitudinal component of the residual stress.

2.1.1. Acustoelastic coefficient

Any welding process results in zones with different microstructural characteristics. To consider the effect of the microstructure in the ultrasonic wave propagation, the acoustoelastic coefficient and indeed the modulus of elasticity have to be experimentally determined for each zone. Thus, samples from that region were removed from the welded plate by water jet cutting and were subjected to a uniaxial tensile test, within the elastic regime. Fig. 5 shows the scheme for obtaining the samples and placement of each one on the universal tensile machine.

The yield strength and ultimate strength for 7050-T7451 aluminum are 470 MPa and 525 MPa respectively (values provided by the material's vendor). The maximum load during the test

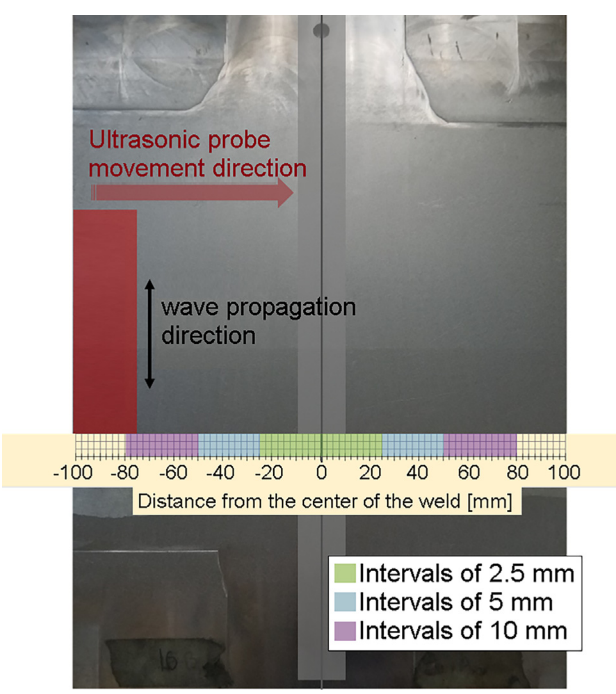

Fig. 4. Measurement positions on the welded plate.

was 20 kN which, does not allow the stress to exceed 50% of the alloy yield strength, with measurements made at each 2 kN. The acoustoelastic coefficient (L) is determined from the slope of the linear relationship of Stress vs $E\Delta t/t_{ref}$, where Δt represents the difference between the TOF for each loading increment and the TOF measured at the zero stress condition. The same test is used to find the Young's modulus, but in this case the measurements are made with a strain gauge and a quarter-bridge circuit. So, the Young's modulus is the ratio of stress to strain for each sample.

All coefficients found are evaluated using the analysis of variance (ANOVA), which is used to find if the variation of microstructure is relevant.

3. Results and Discussion

In this section, a brief material characterization is presented, followed by results of the calibration experiments and the residual stresses determination using the ultrasonic method. Then, a quality index is proposed and discussed.

3.1. Material characterization

Figure 6 shows a macrography of the weld cross-section. For FSW, it is known that 3 constituent zones could be distinguish in addition to the base material (BM), which are the heat-affected zone (HAZ), the thermomechanically affected zone (TMAZ) and the stir zone or nugget (NZ).

The NZ is characterized by containing fine-sized recrystallized grains that roughly coincide with the shape of the welding tool, while the TMAZ region presents highly deformed grains. For the 7050-T7451 aluminum joints evaluated, the deformed grains also extend to the central zone.

Micro-hardness was determined for the cross section of the weld at three depths from the surface: top (0.5 mm from the top surface), middle (2.5 mm from the surface) and bottom (0.5 mm from the bottom surface), Figure 7.

For heat-treatable aluminum alloy, the dissolution of precipitates under temperature increase reduces the hardness of the affected zones. The parent material exhibit a mean hardness of from 169 HV that decreases up to a minimum value close to 150 HV for the top and around 145 for middle and bottom. Minimum hardness corresponds to the shape through depth. For the TMAZ and NZ the hardness increases, reaching local maximum values around 167 HV and a local minimum of 161 HV, at the center.

This cross-section micro-hardness distribution is characteristic of other FSW joints reported in several studies [39–41]. Particularly, the hardness decreasing was not drastic as in other cases reported for similar alloys [42].

3.2. Preliminary and calibration experiments

To consider the effect of the metallographic properties of the zones formed by the weld on ultrasonic wave velocity, Young's modulus and acoustoelastic coefficient were determined from representative samples. Fig. 8 shows the stress–strain curve for the elastic region for each of them.

Notice that the values are a little bit lower than those cited in metals handbooks. This probably happens because non-standard samples were used for the tests. The width of the samples covers more than one welding region, and the non-uniformity structure can affect the elasticity of the material. The sample geometry was defined as a function of the size of the ultrasonic probe available for further determination of the acoustoelastic coefficient. Besides, this can be a characteristic of the plate from where the samples where cut.

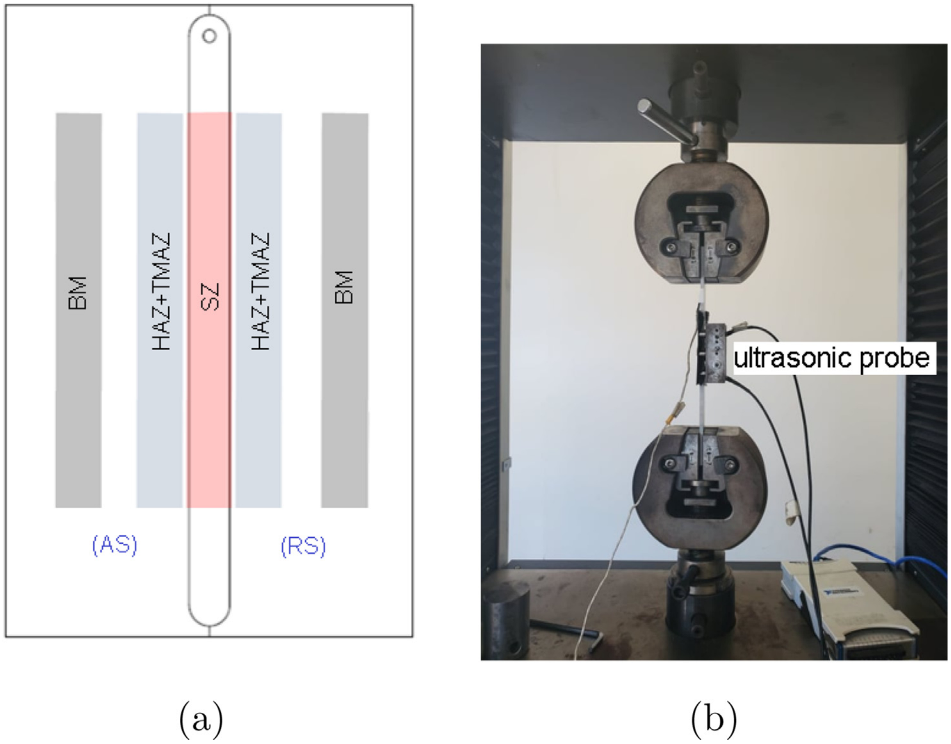

Fig. 5. a) Sample sketch, (b) Tensile test for acoustoelastic coefficient determination.

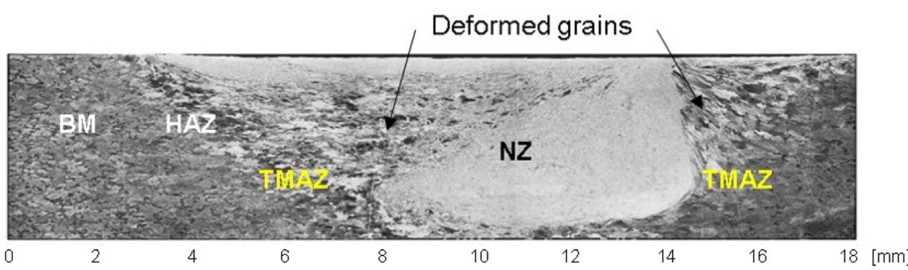

Fig. 6. Optical macrograph for the cross-section of a FSW joint of 7050-T7451 aluminum alloy.

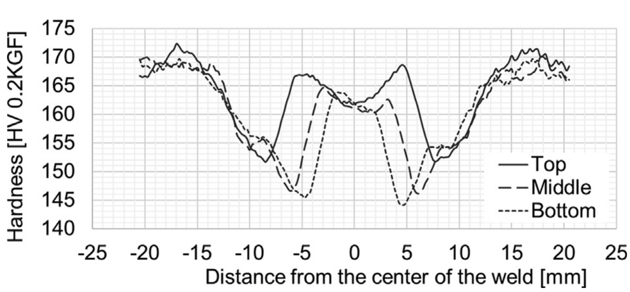

Fig. 7. Micro-hardness distribution along the weld transversal axis on the cross-section.

A single-factor analysis of variance (ANOVA) applied to all obtained values can be seen in Table 2. The F test statistic is lower than the F critical; consequently, the means of the groups can be considered equal. In this way, Young's modulus calculated as the average of all values found experimentally in the tested samples can represent the behavior of the material in any region.

Thus, to find the acoustoelastic coefficient, the same Young's modulus is used for all AA7050 samples, regardless of the metallographic region they represent.

The relationship between the applied stress and the term that includes the TOF measured during the tensile test for different sample types from the same plate is shown in Fig. 9. Notice that the relationship is linear, so the slope represents the acoustoelastic coefficient.

The same test is repeated on samples from other plates. The acoustoelastic coefficients found for samples of the same type from different plates were equal because of the F test $<$ F critical in all cases. However, the variation of the acoustoelastic coefficient of different sample types but from the same plate does not repeat the uniformity statement; for one plate, the F value was higher than the F critical. Considering this situation, the ANOVA is performed on all experimentally values for each plate (P3, P6 and P7), Table 3. According to the F test, the hypothesis that values are equal is verified again; therefore, it is possible to use the average of all results, as the acoustoelastic coefficient for all plates.

To resume, it was demonstrated that the influence of metallographic characteristics on the elastic properties of the 7050 aluminum alloy welded by FSW is low and can be disregarded. Considering that not all base material was recrystallized in the NZ (Figure 6), this assumption is justified. Thus, unique values of 65583 MPa and 2.95 for Young's modulus and acoustoelastic coef-

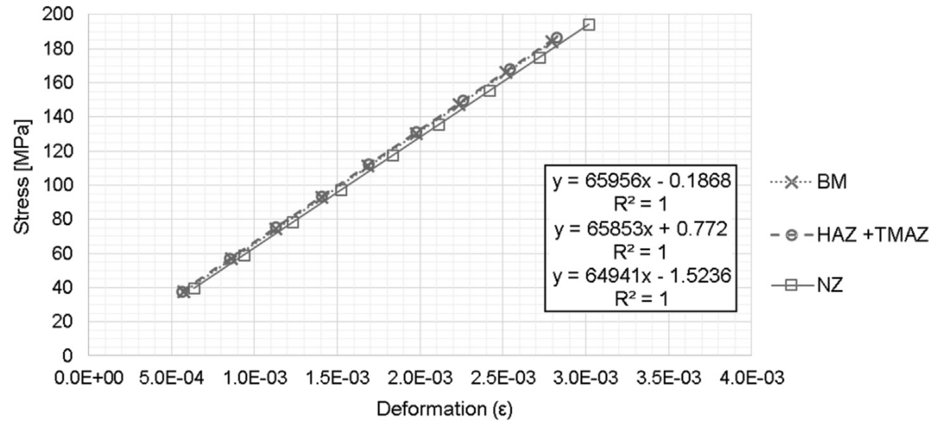

Fig. 8. Stress–strain curve for 7050 aluminum alloy, elastic region.

Table 2
ANOVA for Young's modulus determination.

Groups	Count	Sum	Mean	Variance		Total average
BM	3	197868	65956	452244		65583
HAZ + TMAZ	3	197559	65853	106837		
SZ	3	194824	64941	25169		
Sources	SS[a]	*df*[a]	MS[a]	F[a]	P-value[a]	F critical[a]
Between Groups	1871294	2	935647	4.8043	0.0568	5.1433
Within Groups	1168501	6	194750			
Total	3039794	8				

Note: Statistical values like Sum, Mean and Total Average are in MPa.
[a] SS: Sum of Squares, *df*: degrees of fredom, $MS = SS/df$, for more details see [43].

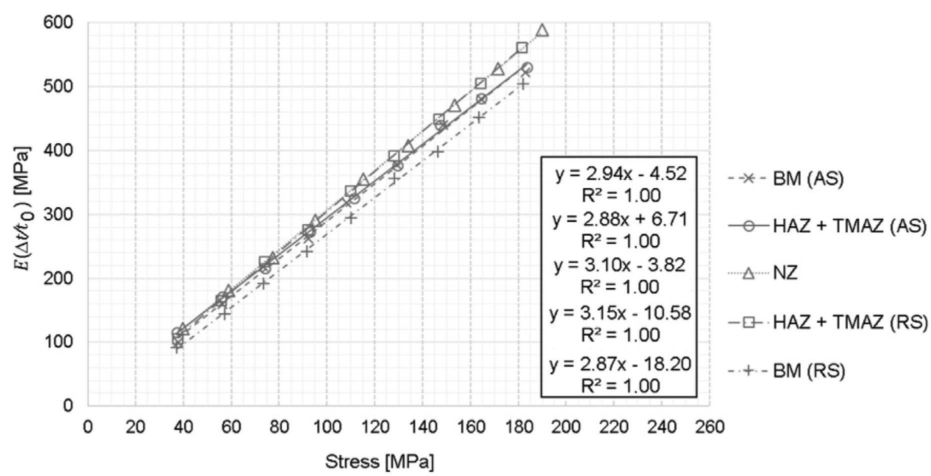

Fig. 9. Acoustoelastic coefficient for 7050 welded aluminum alloy.

Table 3
ANOVA for Acoustoelastic Coefficient determination.

Groups	Count	Sum	Mean	Variance		Total average
P3	15	43.56	2.90	0.0154		2.95
P6	11	32.73	2.98	0.0201		
P7	11	32.71	2.97	0.0239		
Sources	SS[a]	*df*[a]	MS[a]	F[a]	P-value[a]	F critical[a]
Between Groups	0.0451	2	0.0226	1.1703	0.3223	3.2759
Within Groups	0.6552	34	0.193			
Total	0.7003	36				

[a] SS: Sum of Squares, *df*: degrees of fredom, $MS = SS/df$, for more details see [43].

ficient are used to determine the residual stresses across the entire plate.

The influence of temperature was considered through a correction factor (f_{temp}) based on the relationship between TOF and plate temperature, Fig. 10. Note that this relationship is linear, so f_{temp} is estimated from the slope and is equal to 2.79 ns/°C. In terms of stress, it represents 12 MPa/°C, approximately; considering that the method tolerance is up to 20 MPa, a variation of 1°C in the plate would not represent a very high influence and so small temperature variations can also be disregarded.

3.3. Residual Stress

The longitudinal residual stresses in the 7050 aluminum plates were determined with the elastic parameters experimentally obtained and the stress-free TOF measured in the plates before welding. The distribution across the weld for two plates are presented in Figs. 11.

Fig. 12 shows the distributions of the remaining plates grouped and presented in a 3D and contour graph. They are organized as the ratio between rotational and traverse speed (R/T), also known as pitch.

The TOF maximum dispersion between repetitions was 5 ns, which for aluminum 7050 represents 20 MPa. This is a very low value compared to the magnitude of tensile strength and it is according to the expected precision for the technique. Plates welded with the same parameters showed similar stress distribution, slightly following the M shape in some cases, as was reported by other authors [30,44]. Maximum values are more concentrated in the middle of the weld, with magnitudes between 149 MPa and 356 MPa. The width of the central crest extends between −12.5 mm and 12.5 mm, covering an area slightly larger than the SZ. In 12.b, it is also possible to see that the intensity of the calculated residual stress is related to the size of the welding zones. Besides, there is a small concentration of high residual stress for low pitch values. A smaller pitch corresponds to a slower rotation and higher traverse speed, which usually represent a combination of parameters for a colder joint.

The height of the inflection before the central crest in Fig. 11 is greater on the advancing side (AS); indeed, most of the residual stresses measured for symmetrical positions on each side of the plate are bigger in AS. Divergences between the estimated stresses at the same position for different plates welded with the same parameters are more noticeable in the BM; this is probably due

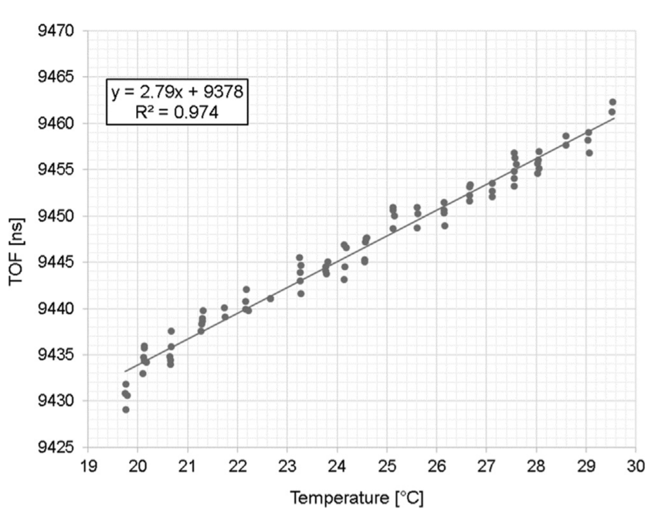

Fig. 10. TOF of the LCR wave as a function of temperature.

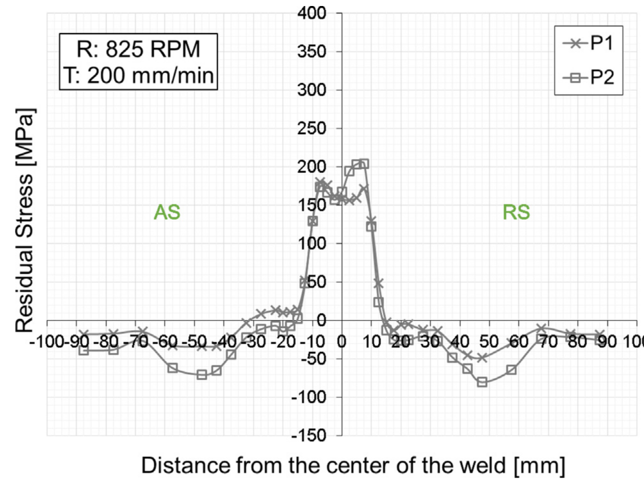

Fig. 11. Longitudinal residual stress distribution in 7050 aluminum alloys.

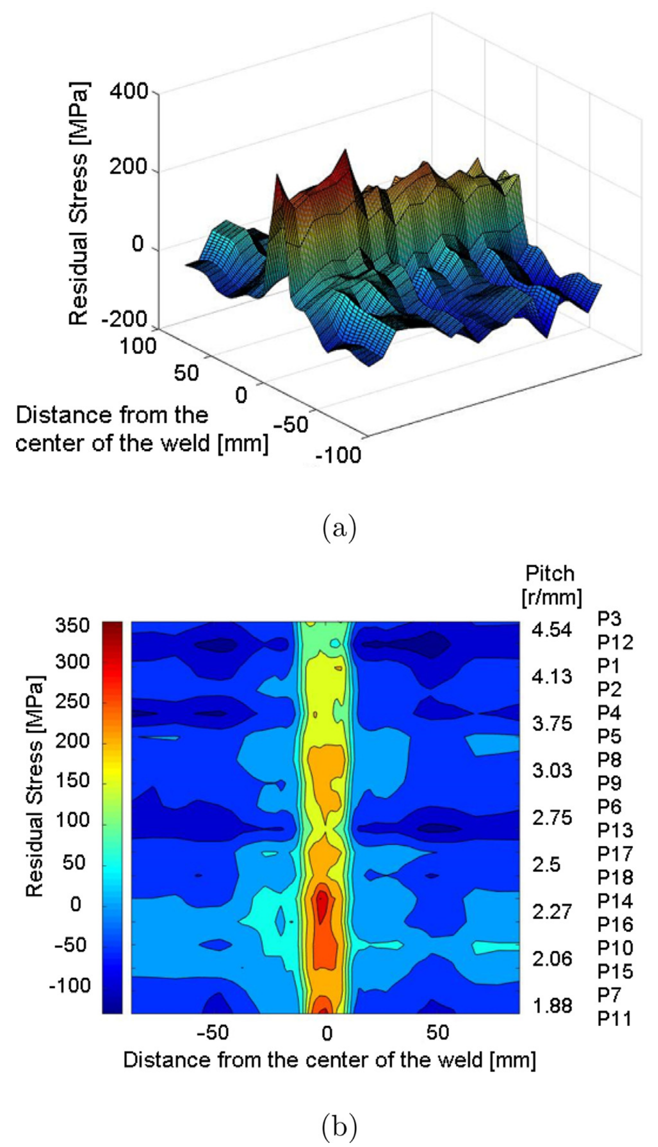

Fig. 12. Longitudinal residual stress distribution for all 7050 aluminum welded plates. (a) 3D surface graph. (b) 2D contour plot.

to the clamping of the plates in the machine that is adjusted manually. The measurement positions in that zone were more widely spaced. Another interesting characteristic for the residual stresses distribution is the presence of a peak in the middle of the weld (e.g. in P14). The tool penetration adjustment was fulfilled by controlling the downward axial force instead of the position, so a small thickness variation could produce greater stresses.

3.4. Quality Index

The residual stress distribution can be difficult to relate to the FSW parameters, so a parameter defined as the equivalent residual stress (ERS) is proposed. The idea is to consider it as a Quality Index for FSW joints, based on the residual stress distribution after the welding.

The ERS is calculated as the average of all stress values in the SZ region, from −10 mm to 10 mm of distance from the center of the weld. Table 4 presents the previous results organized according to the variables R and T. The table shows that the higher traverse speed (T), the higher the residual stress level. Otherwise, the rotational speed (R) does not appear to have that much influence on the magnitude of the ERS.

A surface map was developed to help to visualize the effects. It shows the mean ERS magnitude of the plates welded with the same combination parameters when compared to the ERS average magnitude, Fig. 13). As can be seen in Fig. 13.b, if the traverse speed increases, ERS also increases. The tool rotations seems to have an opposite effect, depending on the traverse speed. For higher T, ERS increases with R; for lower T, ERS decreases with R. That is why the R influence is not so clear in the whole process.

Since all joints have proven to be free from welding defects or distortions, the process quality can be associated with the stress distribution. Thus, an alternative to improve the process, considering the level of residual stresses produced by welding, is to reduce the tool traverse speed at a high rotational speed. That selection of parameters conducts to lower residual stress. In short, the lower the ERS, the higher the resulting quality.

The behavior described is justified by the formability of the 7050 aluminum alloys. As they are straightened by heat treatment, any increment in temperature can affect their mechanical properties. The temperature increment can induce the formation and growth of precipitates in the affected zones, producing localized hardening. The degree of this growth decreases with the reduction of time above a critical temperature, which can be obtained with an increase in the welding advance speed or traverse speed for FSW. Hardness has an inverse relationship to residual stress. Hence, higher speeds produces lower growth of precipitates, which results in less hardness and, therefore, higher residual stress.

The maximum magnitude found for the proposed index (ERS) was approximately 250 MPa, which corresponds to 50% of the material's yield strength. Furthermore, instead of using the ERS as a quality criterion, it is possible to use the inverse of the ERS value multiplied by the material's yield strength, in MPa. This new format can be quite convenient for the analysis.

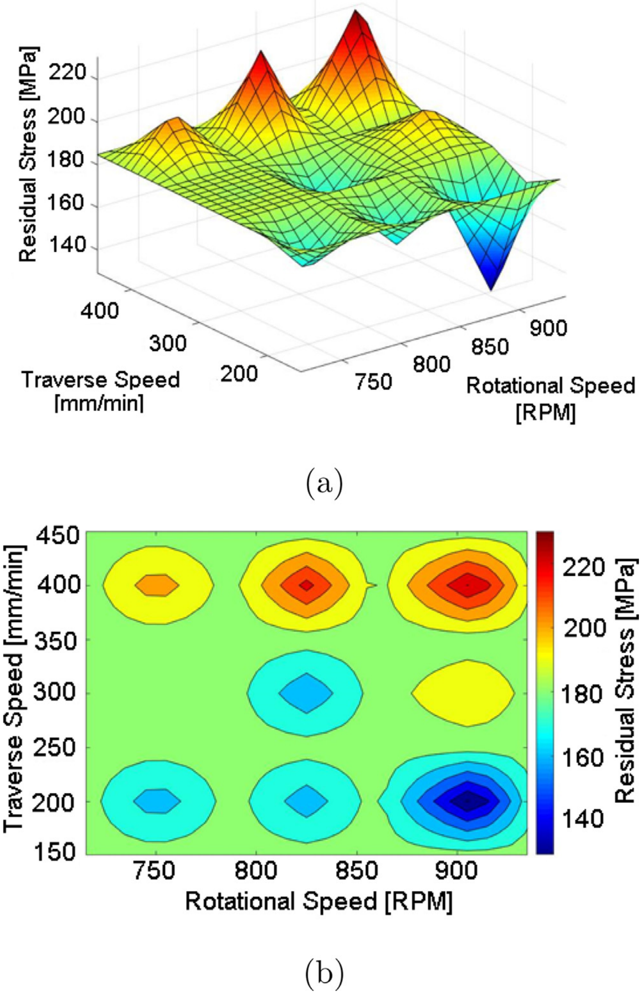

Fig. 13. Relationship between Equivalent Residual Stress (ERS) and FSW parameters for 7050 aluminum alloy. (a) Surface graph. (b) Contour graph.

Table 5 shows the proposed dimensionless parameter, which we can call the quality index (QI-FSW). Using this index, the smallest number refers to the worst quality plate (908 RPM and 400 mm/min); and the best one would be the plate welded with 908 RPM and 200 mm/min.

In summary, both the dimensionless indexes, the ERS of Table 4 and the IQ-FSW of Table 5 can be used to evaluate the quality of the FSW process applied to this aluminum alloy. Considering that all the residual stress profiles presented similar behavior, the indexes proposed are more convenient to interpret and use, fulfilling the purpose of this work.

Table 4
Equivalent Residual Stress (ERS) for all 7050 aluminum welded plates.

	Rotate Speed (R) RPM		
Traverse Speed (T) mm/min	750	825	908
200	173.66	158.26	107.07
	152.28	169.10	144.03
300	171.56	138.84	185.43
	197.49	183.56	213.90
400	218.91	217.35	220.40
	194.49	230.77	246.58

Note: Equivalent Residual Stress (ERS) values are in MPa.

Table 5
Dimensionless quality index for all 7050 aluminum welded plates.

Traverse Speed (T) mm/min	Rotate Speed (R) RPM 750	825	908
200	2.71	2.97	4.39
	3.09	2.78	3.26
300	2.74	3.39	2.53
	2.38	2.56	2.20
400	2.15	2.16	2.13
	2.42	2.04	1.91

4. Conclusion

This work studied the viability of quantifying the stresses generated in joints of Aluminum welded with the FSW process employing ultrasonic Lcr waves. The study aims to find an NDT way to inspect the propensity to failures in welds without detectable defects from the process while searching for the best welding parameters. The main conclusions are:

- The quality indexes, ERS and QI-FSW, show to be adequate for the task. Both indicate the best combination of welding parameters and quantify the propensity to failure, through the measuring of the stresses.
- The low data dispersion found in all ultrasonic experiments shows that the technique is adequate for residual stresses determination, as or more precise than other destructive techniques. Some repeatability disagreements between plates welded with the same characteristics can be attributed to the FWS process. It is possible that the process could be better controlled with some additional welding machine adjustments. This can be done for any particular setup and machine in any welding site.
- The ultrasonic method had the same order of magnitude of related work, as expected. Their distribution follows the profile described in the literature: maximum residual tensile stresses in the stir zone, decreasing as they are located away from the center of the weld.
- For the metallographic characteristics of the zones created by the welding processes, it was shown that these do not significantly affect the variation of the ultrasonic wave velocity. Therefore, we can use the same elastic properties for determining the residual stresses throughout the entire welded plate.

Concluding, the next step of this research should be testing the propensity to failure of the plates welded in some of the conditions evaluated in this work through static and fatigue conditions. This is necessary because, so far, we supposed that the stress is the only factor to warranty the safety in a perfect joint, with no identified defects. That is a defendable hypothesis since it is used with most of the mechanical failure analysis of uniform materials. However, this is not the case with a welding joint. Thus, more can be found on the relation among failures, stresses, and material uniformity for aluminum 7050 FSW joints. Notwithstanding, considering or not that our hypothesis is valid, this work showed an important contribution to the development of an NDT method to evaluate the quality of FSW joints.

5. Data availability

The raw/processed data required to reproduce these findings cannot be shared at this time due to technical or time limitations.

Data availability

Data will be made available on request.

Declaration of Competing Interest

The authors declare that they have no known competing financial interests or personal relationships that could have appeared to influence the work reported in this paper.

Acknowledgments

The authors acknowledge the financial support given by CAPES and from the São Paulo Research Foundation, FAPESP (Fundação de Amparo à Pesquisa de São Paulo), Grant No. 2018/18546–3. Thanks to Lightweight Structures Laboratory (LEL) at the Institute for Technological Research (IPT) in Brazil, especially Andre Ferrara Carunchio and Mario Batalha, for the welding performance. This research used facilities of the Brazilian Center for Research in Energy and Materials (CNPEM) with the collaboration of Itamar Neckel, Daniel Yukio Kakizaki and Rafael Defavari. Shirley Garcia is also grateful to SENESCYT (Secretaría de Educación Superior, Ciencia, Tecnología e Innovación), Grant Funding No. 2015-AR2Q8297 and to the Ecuadorian company INTEG S.A.

References

[1] A. Tiwary, R. Kumar, J.S. Chohan, A review on characteristics of composite and advanced materials used for aerospace applications, Mater. Today: Proc. 51 (2022) 865–870, https://doi.org/10.1016/j.matpr.2021.06.276.
[2] G. Kastratović, A. Grbović, A. Sedmak, Ž. Božić, S. Sedmak, Composite material selection for aircraft structures based on experimental and numerical evaluation of mechanical properties, Proc. Struct. Integr. 31 (2021) 127–133, https://doi.org/10.1016/j.prostr.2021.03.021.
[3] T. Devezas, Trends in aviation: rebound effect and the struggle composites x aluminum, Technol. Forecast. Soc. Chang. 160 (2020) 120241, https://doi.org/10.1016/j.techfore.2020.120241.
[4] W. Thomas, E. Nicholas, Friction stir welding for the transportation industries, Mater. Des. 18 (4–6) (1997) 269–273, https://doi.org/10.1016/s0261-3069(97)00062-9.
[5] B. Zhou, B. Liu, S. Zhang, The advancement of 7xxx series aluminum alloys for aircraft structures: A review, Metals 11 (5) (2021) 718, https://doi.org/10.3390/met11050718.
[6] J. Staley, Aging kinetics of aluminum alloy 7050, Metall. Trans. 5 (4) (1974) 929–932, https://doi.org/10.1007/BF02643150.
[7] M. Ashjari, A. Feizi, 7xxx aluminum alloys; strengthening mechanisms and heat treatment: a review, Mater. Sci. Eng. Int. J. 2 (2) (2018) 49–53, https://doi.org/10.15406/mseij.2018.02.00034.
[8] A. Azarniya, A.K. Taheri, K.K. Taheri, Recent advances in ageing of 7xxx series aluminum alloys: a physical metallurgy perspective, J. Alloy. Compd. 781 (2019) 945–983, https://doi.org/10.1016/j.jallcom.2018.11.286.
[9] S. Gupta, R.S. Haridas, P. Agrawal, R.S. Mishra, K.J. Doherty, Influence of welding parameters on mechanical, microstructure, and corrosion behavior of friction stir welded al 7017 alloy, Mater. Sci. Eng.: A (2022) 143303, https://doi.org/10.1016/j.msea.2022.143303.
[10] J.P. Oliveira, J. Shen, J. Escobar, C. Salvador, N. Schell, N. Zhou, O. Benafan, Laser welding of h-phase strengthened ni-rich niti-20zr high temperature shape memory alloy, Materials & Design 202 (2021) 109533.
[11] T. Chen, Process parameters study on FSW joint of dissimilar metals for aluminum–steel, Journal of materials science 44 (10) (2009) 2573–2580, https://doi.org/10.1007/s10853-009-3336-8.

[12] P. Threadgill, A. Leonard, H. Shercliff, P. Withers, Friction stir welding of aluminium alloys, Int. Mater. Rev. 54 (2) (2009) 49–93, https://doi.org/10.1179/174328009X411136.
[13] H. Lombard, D. Hattingh, A. Steuwer, M. James, Effect of process parameters on the residual stresses in AA5083-H321 friction stir welds, Materials Science and Engineering: A 501 (1–2) (2009) 119–124, https://doi.org/10.1016/j.msea.2008.09.078.
[14] A. Janeczek, J. Tomków, D. Fydrych, The influence of tool shape and process parameters on the mechanical properties of aw-3004 aluminium alloy friction stir welded joints, Materials 14 (12) (2021) 3244, https://doi.org/10.3390/ma14123244.
[15] J.-Q. Su, T. Nelson, R. Mishra, M. Mahoney, Microstructural investigation of friction stir welded 7050–T651 aluminium, Acta materialia 51 (3) (2003) 713–729, https://doi.org/10.1016/S1359-6454(02)00449-4.
[16] K. Jata, K. Sankaran, J. Ruschau, Friction-stir welding effects on microstructure and fatigue of aluminum alloy 7050–T7451, Metallurgical and materials transactions A 31 (9) (2000) 2181–2192, https://doi.org/10.1007/s11661-000-0136-9.
[17] R. Brown, W. Tang, A.P. Reynolds, Multi-pass friction stir welding in alloy 7050–T7451: Effects on weld response variables and on weld properties, Materials Science and Engineering: A 513 (2009) 115–121, https://doi.org/10.1016/j.msea.2009.01.041.
[18] K. Xiao, P. Liu, S. Sun, W. Guo, S. Li, J. Hu, H. Zhang, Study on fatigue crack propagation and fracture characterization of 7050–t7451 friction stir welded joints, J. Mater. Eng. Perform. 30 (8) (2021) 5625–5632, https://doi.org/10.1007/s11665-021-05797-y.
[19] G. Webster, A. Ezeilo, Residual stress distributions and their influence on fatigue lifetimes, Int. J. Fatigue 23 (2001) 375–383, https://doi.org/10.1016/S0142-1123(01)00133-5.
[20] H. Liu, H. Fujii, M. Maeda, K. Nogi, Tensile properties and fracture locations of friction-stir-welded joints of 2017–T351 aluminum alloy, Journal of materials processing technology 142 (3) (2003) 692–696, https://doi.org/10.1016/S0924-0136(03)00806-9.
[21] N. Tebedge, G. Alpsten, L. Tall, Residual-stress measurement by the sectioning method, Experimental mechanics 13 (2) (1973) 88–96, https://doi.org/10.1007/BF02322389.
[22] J. Lu, Handbook of measurement of residual stresses, Fairmont Press (1996).
[23] M. Beghini, L. Bertini, Recent advances in the hole drilling method for residual stress measurement, J. Mater. Eng. Perform. 7 (2) (1998) 163–172, https://doi.org/10.1361/105994998770347882.
[24] A. Allen, M. Hutchings, C. Windsor, C. Andreani, Neutron diffraction methods for the study of residual stress fields, Adv. Phys. 34 (4) (1985) 445–473, https://doi.org/10.1080/00018738500101791.
[25] X-ray diffraction residual-stress techniques, in: Materials Characterization, ASM International, 2019, pp. 440–458. doi:10.31399/asm.hb.v10.a0006632.
[26] C. Ruud, A review of selected non-destructive methods for residual stress measurement, NDT international 15 (1) (1982) 15–23, https://doi.org/10.1016/0308-9126(82)90083-9.
[27] D. Egle, D. Bray, Measurement of acoustoelastic and third-order elastic constants of rail steel, The Journal of the Acoustical Society of America 59 (S1) (1976), https://doi.org/10.1121/1.2002636. S32–S32.
[28] E. Tanala, G. Bourse, M. Fremiot, J. De Belleval, Determination of near surface residual stresses on welded joints using ultrasonic methods, NDT & E International 28 (2) (1995) 83–88, https://doi.org/10.1016/0963-8695(94)00013-A.
[29] H. Qozam, S. Chaki, G. Bourse, C. Robin, H. Walaszek, P. Bouteille, Microstructure effect on the Lcr elastic wave for welding residual stress measurement, Exp. Mech. 50 (2) (2010) 179–185, https://doi.org/10.1007/s11340-009-9283-0.
[30] I. Hadji, R. Badji, M. Gaceb, N. Kherrouba, L. Rabahi, Investigation of the effect of aluminum alloy position on residual stresses in dissimilar fsw weld by using the ultrasonic method, IOP Conference Series: Materials Science and Engineering 461 (2018) 012022, https://doi.org/10.1088/1757-899x/461/1/012022.
[31] Y. Javadi, H. Salimi Pirzaman, M. Hadizadeh Raeisi, M. Ahmadi Najafabadi, Ultrasonic evaluation of welding residual stresses in stainless steel pressure vessel, J. Pressure Vessel Technol. 135 (4) (2013), https://doi.org/10.1115/1.4023432.
[32] H. Liu, Y. Li, T. Li, X. Zhang, Y. Liu, K. Liu, Y. Wang, Influence factors analysis and accuracy improvement for stress measurement using ultrasonic longitudinal critically refracted (lcr) wave, Appl. Acoust. 141 (2018) 178–187, https://doi.org/10.1016/j.apacoust.2018.07.017.
[33] W. Wang, C. Xu, Y. Zhang, Y. Zhou, S. Meng, Y. Deng, An improved ultrasonic method for plane stress measurement using critically refracted longitudinal waves, NDT & E International 99 (2018) 117–122, https://doi.org/10.1016/j.ndteint.2018.07.006.
[34] N. Ning, et al., Ultrasonic inspection of s line of 7050 aluminum alloy friction stir welding, in: International Conference on Mechanical Engineering, Measurement Control, and Instrumentation, Vol. 11930, SPIE, 2021, pp. 575–581. doi:10.1117/12.2611104.
[35] M. Tabatabaeipour, J. Hettler, S. Delrue, K. Van Den Abeele, Non-destructive ultrasonic examination of root defects in friction stir welded butt-joints, Ndt & E International 80 (2016) 23–34, https://doi.org/10.1016/j.ndteint.2016.02.007.
[36] S.A. Garcia Ruano, et al., Tensões residuais medidas por acustoelasticidade em juntas de ligas de alumínio soldadas por atrito e mistura linear (fsw), Ph.D. thesis (2021).
[37] D.S. Hughes, J. Kelly, Second-order elastic deformation of solids, Physical review 92 (5) (1953) 1145, https://doi.org/10.1103/physrev.92.1145.
[38] Z. Abiza, M. Destrade, R.W. Ogden, Large acoustoelastic effect, Wave Motion 49 (2) (2012) 364–374, https://doi.org/10.1016/j.wavemoti.2011.12.002.
[39] C. Sharma, V. Upadhyay, V. Verma, A. Tripathi, S. Sharma, Tensile behaviour of friction stir welded joints of different aluminium alloys, Journal of Engineering Research (2021), https://doi.org/10.36909/jer.ICCEMME.15693.
[40] S. Gachi, M. Aissani, F. Boubenider, Temperature evolution, microstructure and mechanical properties of heat-treatable aluminum alloy welded by friction stir welding: Comparison with tungsten inert gas, International Journal of Materials and Metallurgical Engineering 12 (11) (2018) 600–604.
[41] I. Morozova, A. Obrosov, A. Naumov, A. Królicka, I. Golubev, D.O. Bokov, N. Doynov, S. Weiß, V. Michailov, Impact of impulses on microstructural evolution and mechanical performance of al-mg-si alloy joined by impulse friction stir welding, Materials 14 (2) (2021), https://doi.org/10.3390/ma14020347.
[42] A. Rodiguez, A. Calleja, L.N. Lopez de Lacalle, O. Pereira, H. Gonzalez, G. Urbikain, J. Laye, Burnishing of fsw aluminum al–cu–li components, Metals 9 (2) (2019) 260, https://doi.org/10.3390/met9020260.
[43] A. Rutherford, Anova and ancova: a glm approach.
[44] X. Xu, H. Yu, Z. Lin, Study of residual stress variation with depth of friction stir welded aluminium plates with different thicknesses, Sci. Technol. Weld. Joining 25 (4) (2020) 297–302, https://doi.org/10.1080/13621718.2019.1693722.